Nanotechnology

TOPICAL REVIEW • OPEN ACCESS

Magnetic domain wall and skyrmion manipulation by static and dynamic strain profiles

OPEN ACCESS
IOP Publishing
Nanotechnology
Nanotechnology 36 (2025) 072003 (16pp)
https://doi.org/10.1088/1361-6528/ad96c2

Topical Review

Magnetic domain wall and skyrmion manipulation by static and dynamic strain profiles

Thomas A Moore

School of Physics and Astronomy, University of Leeds, Leeds LS2 9JT, United Kingdom

E-mail: T.A.Moore@leeds.ac.uk

Received 20 June 2024, revised 27 September 2024
Accepted for publication 25 November 2024
Published 6 December 2024

Abstract

Magnetic domain walls and skyrmions in thin film micro- and nanostructures have been of interest to a growing number of researchers since the turn of the millennium, motivated by the rich interplay of materials, interface and spin physics as well as by the potential for applications in data storage, sensing and computing. This review focuses on the manipulation of magnetic domain walls and skyrmions by piezoelectric strain, which has received increasing attention recently. Static strain profiles generated, for example, by voltage applied to a piezoelectric-ferromagnetic heterostructure, and dynamic strain profiles produced by surface acoustic waves, are reviewed here. As demonstrated by the success of magnetic random access memory, thin magnetic films have been successfully incorporated into complementary metal-oxide-semiconductor back-end of line device fabrication. The purpose of this review is therefore not only to highlight promising piezoelectric and magnetic materials and their properties when combined, but also to galvanise interest in the spin textures in these heterostructures for a variety of spin- and straintronic devices.

Keywords: magnetic domain walls, skyrmions, thin magnetic films, artificial multiferroics, spintronics, straintronics

1. Introduction

Domain walls in continuous and laterally confined magnetic thin film structures have been of interest for many years, both from a fundamental and an applied perspective [1–10]. In confined magnetic structures such as nanostrips, Bloch- or Néel-type [1] or more complex transverse or vortex domain wall spin structures [9, 10] can arise (figure 1(a)), depending on the magnetic anisotropy. Proposed applications of domain walls have included magnetic bubble memory [3], domain wall logic [5, 6], racetrack memory [7], domain wall magnetic random access memory (MRAM) [8], and most recently, unconventional computing schemes [11–14], shown in figure 1, and these ideas have helped to drive fundamental research. The first implemented application was the magnetic multiturn counter using 180° domain walls in a Permalloy film [15]. Chiral domain walls [16] and magnetic skyrmions [17] may arise when a Dzyaloshinskii Moriya interaction (DMI) is present [18], and while they may both be exploited in similar ways to achiral domain walls, they also present potentially useful properties arising from their topology [19–21]. Examples

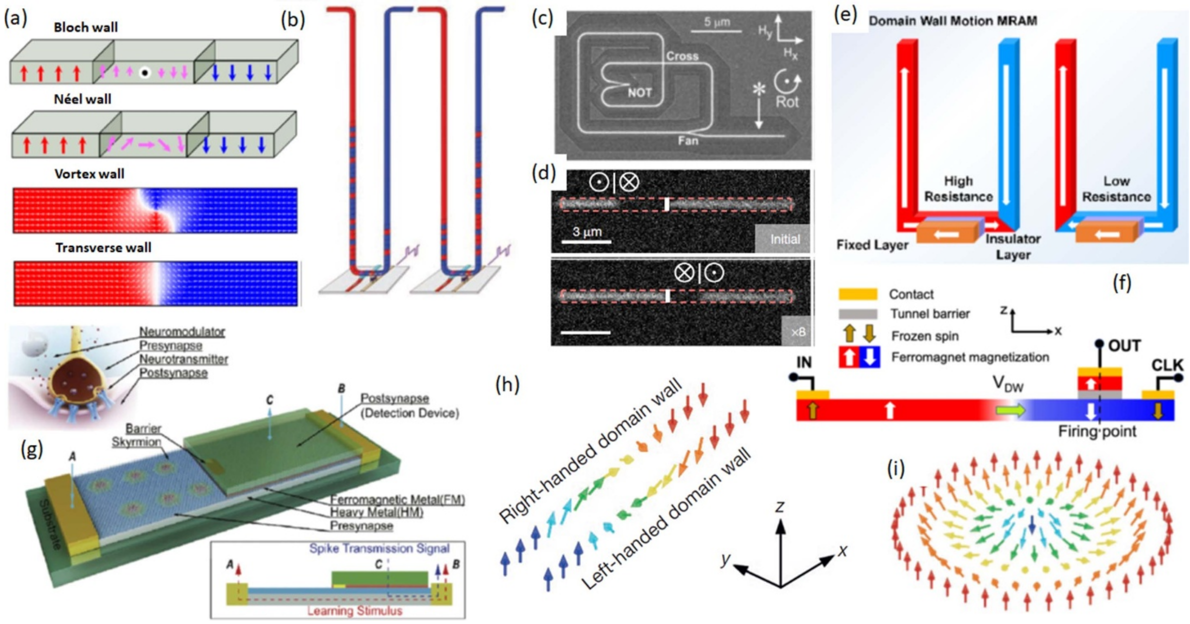

Figure 1. Applications of domain walls and skyrmions. (a) Magnetic domain walls in nanostrips: variation of the magnetization in a Bloch, Néel, vortex and transverse wall. Reprinted from [23], Copyright (2022), with permission from Elsevier. (b) The racetrack memory is a ferromagnetic nanowire, with data encoded as a pattern of magnetic domains. Pulses of spin-polarised current move the domain walls coherently along the length of the wire past read and write elements. A vertical configuration racetrack offers high storage density normal to the plane of the substrate. The two cartoons show the magnetic patterns in the racetrack before and after the domain walls have moved past the read and write elements. From [7]. Reprinted with permission from AAAS. (c) Field-driven magnetic domain wall logic. Focused ion beam image of a magnetic nanowire loop containing a NOT gate, fan-out junction, and cross-over junction. The directions of rotating field components (H_x and H_y), and the sense of field rotation (Rot) are indicated. From [5]. Reprinted with permission from AAAS. (d) Current-driven magnetic domain wall logic. Two magneto-optic Kerr effect images from a sequence of domain wall inversion for a domain wall incident from the left. The edges of the magnetic racetracks are indicated by red dashed lines and the positions of the inverters are shown by white lines. The bright and dark regions correspond to up and down magnetization, respectively. Reproduced from [6], with permission from Springer Nature. (e) MRAM based on domain wall motion. Reprinted from [23], Copyright (2022), with permission from Elsevier. (f) Domain wall—magnetic tunnel junction neuron. Cartoon of the structure of the neuron, with colours and images defined by the legend. Reproduced from [13]. © IOP Publishing Ltd All rights reserved. (g) Schematic of a proposed skyrmionics synaptic device. To mimic a neuromodulator, a bidirectional learning stimulus flowing through the HM from terminal A to terminal B (or vice versa) drives skyrmions into (or out of) the postsynapse region to increase (or decrease) the synaptic weight, mimicking the potentiation/depression process of a biological synapse. Reproduced from [21]. © IOP Publishing Ltd All rights reserved. (h) Schematic of the spin configuration in interfacial-DMI-induced chiral Néel domain walls, with the colour scale corresponding to the out-of-plane (z) magnetization component. Reproduced from [22], with permission from Springer Nature. (i) A Néel-type skyrmion, where the spins rotate in the radial planes from the core to the periphery. Reproduced from [22], with permission from Springer Nature.

of chiral Néel domain walls [22] and a Néel-type skyrmion [22] as envisaged in a magnetic thin film with an interfacial (i-)DMI are shown in figures 1(h) and (i). For the physics of domain walls and skyrmions and their potential applications we refer the reader to earlier texts and reviews [1, 9, 10, 22–30], as the focus of this review is specifically on the manipulation of domain walls and skyrmions by strain.

In many technological schemes, domain walls and skyrmions are moved around a thin film structure using spin torque derived from an electric current flowing in the device. However, an electric current is not the most efficient means of manipulating spin textures, because of inefficiencies in spin polarisation, spin Hall effect and spin injection processes, and because quite high current densities are needed to overcome pinning effects, and, furthermore, these currents lead to energy wasted via Joule heating. For more than a decade it has been recognised that electric fields may be used to influence magnetic properties [31, 32] and could potentially be much more efficient than electric current [33]. Avoiding current flow in the magnetic device typically means either directly gating the magnetic layer [34], manipulating the magnetic properties by charging or ionic transport effects [35–37], or indirectly modulating the magnetic properties via strain from a piezoelectric [38–40]. The strain can be applied either continuously, as a static strain [38–40], or dynamically, in the form of a pulse or an acoustic wave [41, 42]. Figure 2 shows some ways in which strain is applied to magnetic thin films. Here, we shall review progress in the manipulation of domain walls and skyrmions by both static and dynamic strain profiles. We shall focus mainly on piezoelectric strain, rather than the strain generated by thin film/substrate lattice mismatch, thermal effects, bending or pressure cell apparatus. Thus the work we discuss is potentially applicable to microelectronic and spintronic devices utilising artificial heterostructures of magnetic and piezoelectric layers.

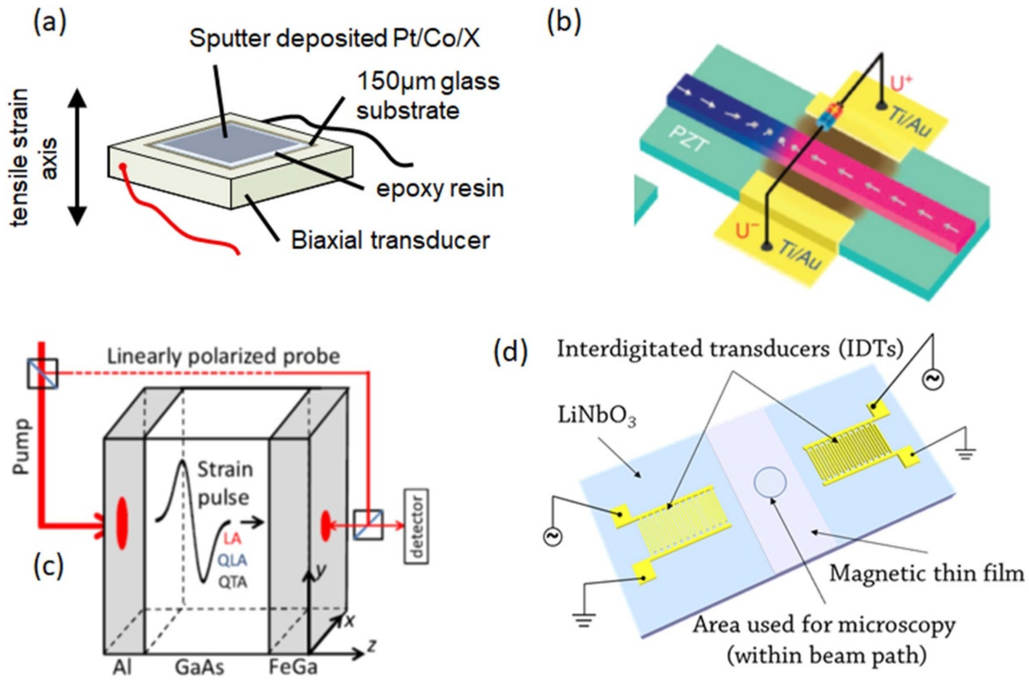

Figure 2. Methods of applying strain to magnetic thin films. (a) Schematic of a thin magnetic film (Pt/Co/X, where X = Pt,Ir) deposited on glass and epoxy bonded to a piezoelectric transducer. (b) Schematic of a ferromagnetic nanowire deposited on a PZT layer. By applying a voltage to electrical contacts (yellow), a local stress is induced, creating a pinning site for a domain wall in the nanowire. Reproduced from [38], with permission from Springer Nature. (c) Schematic of picosecond acoustic pulse generation. Optical pump laser pulses are incident on a 100 nm Al film deposited on GaAs on the opposite side to the film of interest (FeGa). Strain pulses are injected from the Al film into the GaAs substrate, which can be purely longitudinal (LA), or quasi-longitudinal (QLA) and quasi-transverse (QTA), depending on the crystal orientation of the substrate (001) or (311) respectively. Reprinted from [41], with the permission of AIP Publishing. (d) Schematic of surface acoustic wave experiment. A 2 mm-wide thin film is deposited on a lithium niobate substrate. An interdigitated transducer is patterned each side of the thin film to launch the SAWs. Reproduced from [42]. CC BY 4.0.

The review is organised as follows. In section 2 we review the work in which magnetic domains and domain walls in thin films have been directly imaged to understand the effect of piezoelectric strain on them. This includes a wide variety of piezoelectric substrates, thin films with in-plane and perpendicular magnetic anisotropy, and imaging techniques. In section 3 we focus on the influence of strain on domain wall motion in magnetic nanostrips, in section 4 we examine skyrmions under strain, and in section 5 we review relatively recent work using the dynamically changing strain profile of surface acoustic waves (SAW) to manipulate domain walls and skyrmions.

2. Imaging the effect of strain on magnetic domain morphology and domain wall spin structure

Multiferroic heterostructures enable the properties of a thin magnetic film to be controlled by strain from an adjacent piezoelectric such as barium titanate (BTO), lead magnesium niobate-lead titanate (PMN-PT) and lead zirconate titanate (PZT). A review by Bandyopadhyay *et al* [43] summarises recent progress in controlling magnetisation in magnetostrictive films deposited on piezoelectrics. We focus in this section on the domain pattern transfer between piezoelectric and ferromagnetic layer. This enables domain wall locations and spin structures to be determined by the strain coupling.

2.1. Thin films with in-plane magnetic anisotropy

Several different materials have been used in which the ferroelectric domains act as a template for magnetic domains in a layer deposited on top. Earlier this century, Eerenstein *et al* confirmed strain coupling between a BTO substrate and a lanthanum strontium manganite (LSMO) film [44]. This was part of a significant increase in the attention paid to multiferroic materials in general [45, 46], associated with the magnetoelectric effect and its potential for reading and writing in data storage applications. Thin film heterostructures comprising piezoelectric and magnetic layers were studied as well as single-phase multiferroics such as bismuth ferrite (BFO). BFO is of interest because it permits exchange coupling to an adjacent ferromagnetic layer, as an alternative to strain coupling. Experiments on $Co_{90}Fe_{10}$/BFO heterostructures have revealed the imprinting of domains, 180° magnetization reversal by electric field (figure 3(a)), and tracked the dynamics of the magnetoelectric transfer from BFO to CoFe domains [47–51].

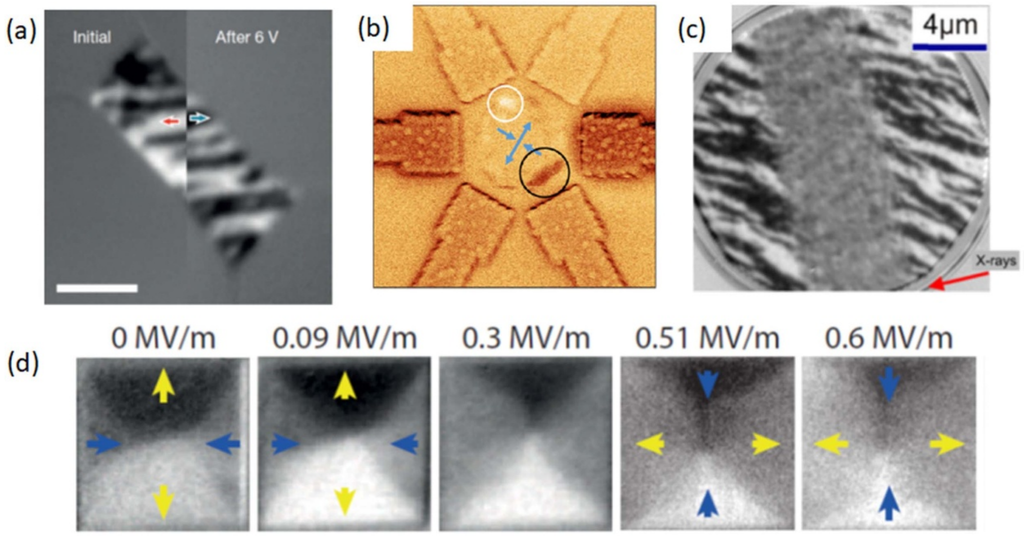

Figure 3. Thin films with in-plane magnetic anisotropy on various ferroelectric and piezoelectric substrates. (a) Initial and final (after 6 V) directions of the in-plane CoFe moments for a CoFe/BFO magnetoelectric device. The XMCD-PEEM images are merged near the centre of the CoFe structure to reveal the magnetisation reversal at each domain. The directions of the magnetisations are highlighted with blue and red arrows. Scale bar is 2 μm. Reproduced from [49], with permission from Springer Nature. (b) AFM image of Ni ring on PZT surrounded by electrodes. Domain walls are shown as black and white spots (circled), and the black domain is larger than the white domain because 25 V has been applied, generating a strain indicated by the blue arrows. The width of an electrode is approximately 500 nm. Reprinted from [52], with the permission of AIP Publishing. (c) XMCD-PEEM image of demagnetized 29 nm thick LSMO/BTO taken at the Mn L_3 edge. White and black contrast indicates magnetization along the x-ray propagation direction. Grey contrast indicates magnetization oblique to the x-ray propagation direction. Reproduced from [53], with permission from Springer Nature. (d) XMCD-PEEM images of a 2 μm wide Ni square, at different applied electric fields. Blue and yellow arrows indicate the directions of the compressive and tensile strains, respectively. Reprinted (figure) with permission from [54], Copyright (2014) by the American Physical Society.

PZT is one of the commonest ferroelectric ceramics; Chung *et al* fabricated thin film PZT with a 100 nm Ni layer on top, separated by a Pt electrode [55]. Stripe domains were imaged in the Ni film by magnetic force microscopy (MFM), and upon applying 10 V (equivalent to an electric field of 7.8 MV m^{-1}) the stripe domain patterns were reversibly altered, due to the generation of in-plane strain in the PZT and coupling of the strain to the Ni layer. To control a single domain, the Ni was patterned into a 35 nm thick nanobar (380 $\times$ 150 nm^2) which at zero electric field was in a single domain state, and with 1.5 V applied (1.2 MV m^{-1}) the single domain transformed into an S-domain state [56]. However, truly local control of magnetic domains can only be achieved by delivering highly localised strain via custom-designed electrode patterns, e.g. to control the position of domain walls in a thin film Ni ring [52] (figure 3(b)). The strain in this instance induces a magnetoelastic anisotropy with the easy axis aligned in the compressive strain direction, and the domain walls subsequently align in this direction too.

PMN-PT is attractive because it has a large d_{33} piezoelectric constant up to around 2000 pC/N, a few times larger than that of PZT. The Landau domain state in Ni squares prepared on a PMN-PT(011) substrate was imaged by photoemission electron microscopy [54]. When 0.6 MV m^{-1} was applied to generate uniaxial in-plane strain, the domains with magnetization in the compressive strain direction grew larger, at the expense of domains with magnetization in the tensile strain direction (figure 3(d)). This amounted to a reversible displacement of the domain walls. Subsequent experiments used PMN-PT to drive domain walls around a Ni ring structure [57], and applied uniaxial stress sequentially along two different noncollinear axes to rotate the magnetization in a Co nanomagnet by 180° [58]. However, these investigations paid little attention to the domains in the piezoelectric component of the heterostructure. For a full understanding, ferroelectric domains must be characterised and this is often done when BTO substrates are used.

BTO can generate strains of order 1% in magnetic epilayers owing to structural phase transitions, larger than that generated by PMN-PT which is typically limited to around 0.2%. Early studies of the LSMO/BTO heterostructure indicated that, while significant magneto-electric coupling was possible, details of the coupling between ferroelectric and magnetic domains at a microscopic level were required to properly understand the results. Chopdekar *et al* [53] investigated the magnetic domain structure of an LSMO thin film epitaxially grown on a BTO substrate using x-ray photoemission electron microscopy and x-ray absorption spectroscopy. It was found that the BTO ferroelectric domain structure imprinted specific domain sizes and wall orientations into the LSMO (figure 3(c)), and that changing the BTO domain structure by cooling from room temperature to 160 K, or by applying an electric field pulse of 10 kV cm^{-1} across the substrate thickness, changed the LSMO domain structure. Domain pattern transfer from BTO, and the temperature and electric field control of the domain structure was also observed in epitaxial Fe [59] and polycrystalline $Co_{60}Fe_{40}$ (figures 4(a)–(d)) [60, 61]

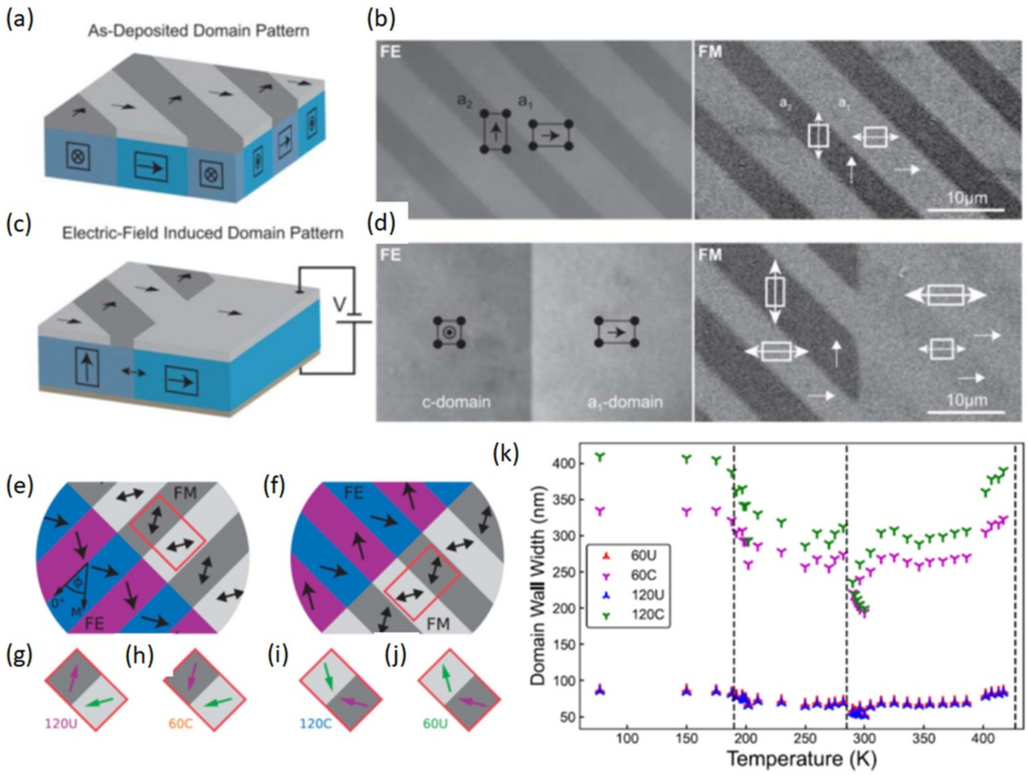

Figure 4. Domain imprinting in CoFe/BTO(100) and Co,CoFeB/BTO(111). (a)–(d) Ferroelectric (FE) and ferromagnetic (FM) microstructure after CoFe film growth on BTO(100) (a), (b) and the application of an out-of-plane electric field of 10 kV cm^{-1} (c), (d). The polarization direction and lattice elongation of the BTO substrate (black rectangles with arrows), the orientation of the strain-induced magnetic easy axis (white rectangles with double-headed arrows), and the magnetization direction in zero applied magnetic field (white arrows) are indicated. Reproduced from [60], with permission from Springer Nature. (e), (f) Sketches of ferroelectric (blue/magenta) and magnetic anisotropy (light/dark grey) domain patterns for a Co film strain coupled to a BTO(111) substrate corresponding to (e) quasiparallel and (f) quasiperpendicular anisotropy patterns. The negative magnetostriction of the Co means that the easy axes of the anisotropy domains in the Co are orthogonal to the polarization in the ferroelectric domains of the BTO. (g)–(j) Possible orientations of the magnetization in the domains leading to four distinct magnetic domain wall structures. Reproduced from [66]. (k) Domain wall width in a CoFeB film on BTO(111) for the various configurations shown in (g)–(j) as a function of temperature. Reproduced from [69].

and Ni films [62]. A BTO(100) substrate was used in all these works, which at room temperature is in the tetragonal phase with a_1–a_2 domains. For the CoFe, when the BTO is cooled to the orthorhombic phase, the uniaxial strain direction and the magnetoelastic easy axes rotate by 90° and on further cooling into the rhombohedral phase, the magnetic domain pattern is preserved in the rotated state [61]. However, when an electric field is applied across the substrate thickness, c-domains with polarisation out-of-plane are generated while the previously imprinted a_1–a_2 stripe pattern is conserved [60]. C-domains may also be formed upon sample cooling through the ferroelectric Curie temperature after film growth [59]. The effect of the deposition temperature of the ferromagnetic layer, whether at room temperature, above T_c, or at an intermediate temperature was analysed by Streubel *et al* [62] for Ni deposited on sc-BTO and it was demonstrated that this influenced the strain-induced anisotropy, with appropriate deposition parameters permitting a local rotation of the magnetic easy axis by 90°. Focusing on the domain walls, it is interesting to note that the width of domain walls in BTO are <5 nm, while the domain walls in a neighbouring ferromagnetic layer with in-plane anisotropy to which they are coupled are typically an order of magnitude wider. It was discovered that the width of 90° domain walls in CoFe elastically coupled to a_1–a_2 domain boundaries in BTO(100) could be tuned by varying an applied magnetic field, and reversibly switched between wide charged and narrow uncharged walls by rotating the applied field [63]. As the magnetic domain walls are pinned to fixed ferroelectric domain boundaries, the magnetization reversal of the ferromagnetic layer is affected [64]. In a $Co_{40}Fe_{40}B_{20}$ film on BTO, Gonzalez *et al* [65] characterised the variation of the domain wall spin structure as a function of magnetic field strength and CoFeB film thickness. Recent studies have investigated the domain pattern transfer between BTO(111) and Co, Ni and CoFeB films [66–69] (figures 4(e)–(k)). Here the imprinted pattern results in 60° and 120° domain walls, which may each be either charged or uncharged depending on the magnetic field history, leading to more options for tailoring the energy landscape of magnetic configurations via field and film thickness.

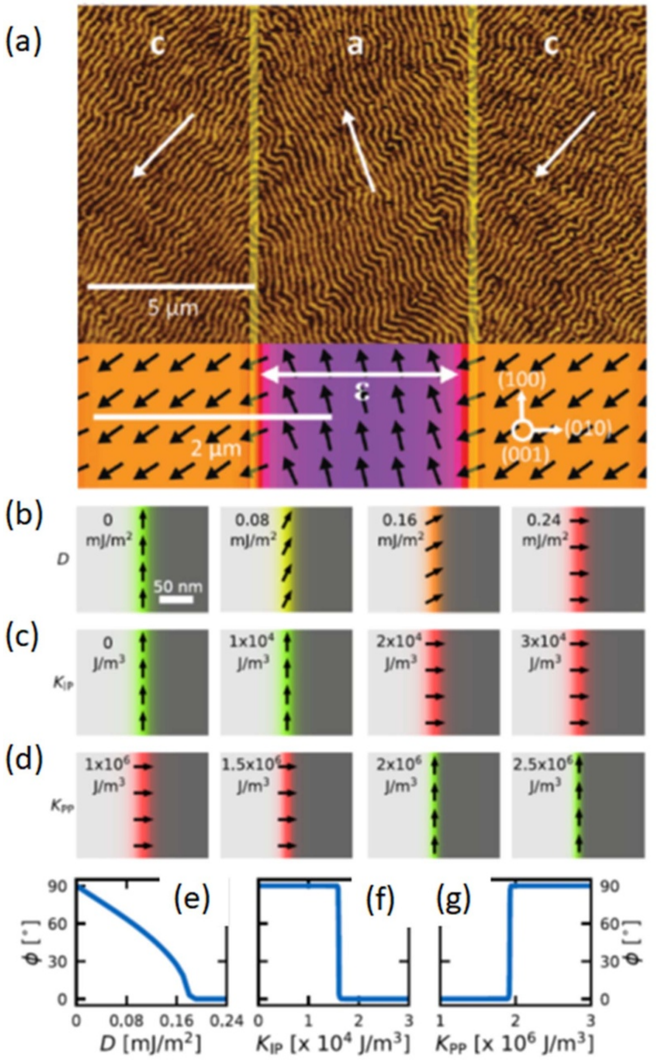

Figure 5. Effect of strain on domain morphology and domain wall spin structure in thin films with perpendicular magnetic anisotropy. (a) Magnetic force microscopy image of tPy/BTO heterostructure after thermal treatment. Ferroelectric domain boundaries between a- and c-domains are indicated by translucent yellow lines. White arrows indicate average stripe domain orientation. The double-headed arrow points along the uniaxial strain direction over the a-domain. Results of in-plane micromagnetic simulation are pictured below. Reprinted from [70], with the permission of AIP Publishing. Simulated images of domain walls as a function of (b) DMI constant D and (c) in plane anisotropy constant K_{IP} for a perpendicular anisotropy constant $K_{PP} = 10^6$ J m^{-3}. (d) Images as a function of K_{PP} for $K_{IP} = 3 \times 10^4$ J m^{-3}. Corresponding domain wall magnetization angles ϕ as a function of (e) D, (f) K_{IP} and (g) K_{PP}. Reprinted (figures) with permission from [71], Copyright (2021) by the American Physical Society.

2.2. Thin films with perpendicular magnetic anisotropy

Thin films with perpendicular magnetic anisotropy (PMA) came to be used in hard disk drives and MRAM because of advantages in data storage density and stability against thermal fluctuations. PMA in technological applications may be a surface effect, where electron orbitals hybridise at interfaces between ultrathin ferromagnetic and non-magnetic layers [72], but it can also arise via perpendicular-to-plane magnetocrystalline anisotropy in thicker $L1_0$-ordered films [73], or an intrinsic perpendicular anisotropy in Ni, Ni-rich NiFe [74] and amorphous rare earth-transition metal alloys [75] once a critical thickness or composition is reached. Fackler *et al* [70] investigated the coupling between the stripe domains that arise in NiFe films (transcritical Permalloy, tPy) due to this intrinsic PMA, and ferroelectric domains in a BTO(001) substrate. An abrupt change in the direction of the magnetic stripe domains was observed at the ferroelectric a–c domain boundaries due to a strain-induced change in in-plane magnetic anisotropy, and the stripe domain period increased when coupled to a ferroelectric a-domain due to a lowering of the out-of-plane magnetic anisotropy energy (figure 5(a)). Ghidini *et al* [76] were able to remove the dominant PMA in Ni films deposited on BTO(001) and thereby erase the stripe domains by cooling the BTO through structural phase transitions, or alternatively by using electric field (0.4 MV m^{-1}) to move ferroelectric domain walls to convert a to c domains. Shirahata *et al* reversibly switched 20 μm wide magnetic stripe domains in Cu/Ni multilayers from out of plane to in plane by applying up to 0.4 MV m^{-1} to the BTO(001) substrate [77], and magnetic domain wall motion was driven by electric field pulses [78]. In the Cu/Ni on BTO, the strain coupling to ferroelastic domains with in-plane and perpendicular polarisation in the BTO causes the formation of domains with perpendicular and in-plane magnetic anisotropy, respectively, in the Cu/Ni multilayer. Magnetic domain walls are elastically pinned to ferroelectric domains walls and so an out-of-plane electric field pulse expands the in-plane magnetic domains. Nucleation and propagation of domain walls in TbFe films were affected by coupling to BTO [79]. Magnetic anisotropy in $L1_0$ FePt was modified by strain from an adjacent shape memory alloy [80]. In thin films with surface anisotropy, PZT has been used to impart strain to Co/Pt and Co/Ni multilayers. A tensile strain of almost 0.1% out-of-plane reduced the perpendicular anisotropy in Co/Pt by approximately 10 kJ m^{-3} and increased the field-driven domain wall creep velocity by 100% [40]. Field-driven domain wall depinning was shown to be enhanced by strain in Co/Ni multilayers, also due to a small reduction in PMA [81]. Interfacial DMI determines the chirality and spin structure of domain walls in thin films with PMA, and anisotropic strain induced by a substrate provided a method of tuning the domain wall spin structure further [82], unlocking Bloch-type chirality. Simulations and modelling have since shown that strain-driven switching between Bloch and Néel domain wall configurations can occur even in the absence of iDMI [71] (figures 5(b)–(g)). In other work, the iDMI was manipulated by strain from a bending apparatus [83], affecting the domain morphology in Co/Pt [84].

3. Domain wall motion in magnetic nanostrips influenced by strain

To investigate the effect of strain on an isolated single magnetic domain wall a laterally confined magnetic strip must be used, rather than a full magnetic film. A strip geometry is also

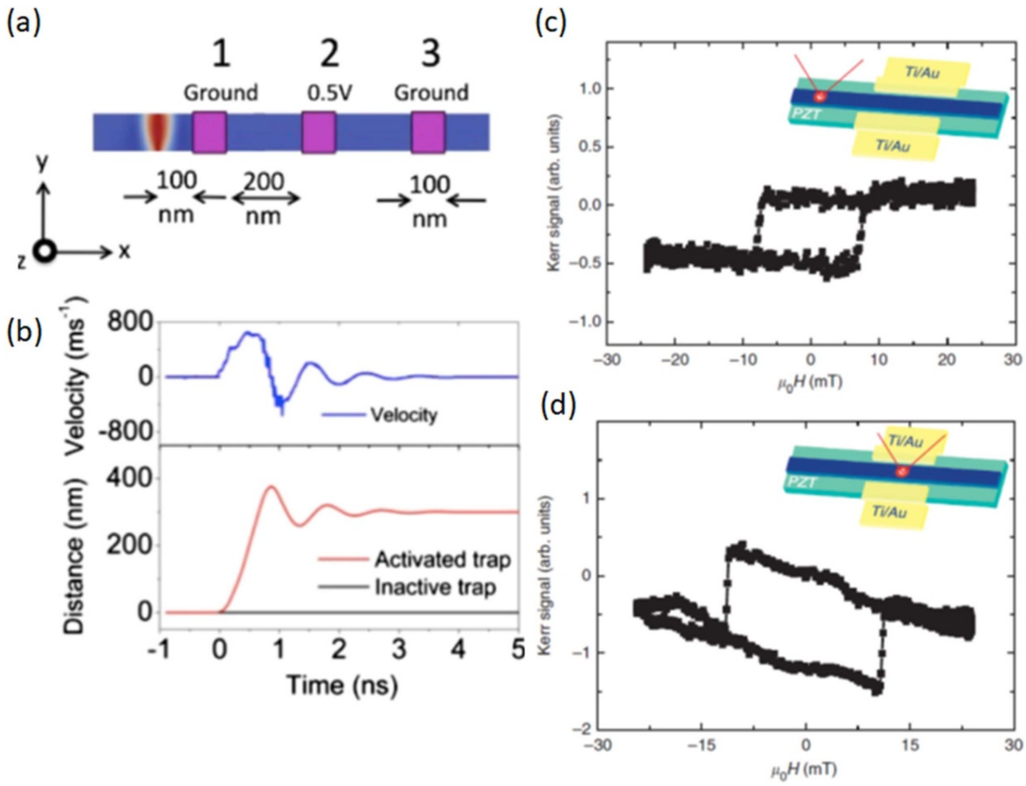

Figure 6. Magnetic nanowires. (a) Schematic of a domain wall trap system, with the domain wall initialised 100 nm from contact 1. (b) The velocity of the domain wall as it moves under the influences of the local stress towards the energy minimum (top) and the movement of a domain wall under the influence of an activated and inactive trap (bottom). Reprinted from [85], with the permission of AIP Publishing. (c) Hysteresis loop determined from a spatially resolved MOKE measurement at a location outside of the PZT electrodes, which indicates a coercive field of 7.5 mT and (d) at a location in between the PZT electrodes, which indicates a coercive field of 11 mT. Insets: illustration of the position of the laser spot used in the MOKE measurement. Reproduced from [38], with permission from Springer Nature.

convenient for applications where individual domain walls are relied upon for sensing or used as data bits. Modelling initially focused on a Permalloy nanowire 5 nm thick and 100 nm wide on a silicon substrate covered with a 200 nm thick layer of PZT [85, 86]. On top of the PZT were a number of 100 nm wide electrical contacts separated by 200 nm used to apply a potential difference and thereby localised strains to the nanowire (figures 6(a) and (b)). These strains were shown to pin domain walls, and furthermore, by applying potentials to contacts in an ordered way, a domain wall could be made to move progressively along the nanowire without the need for a magnetic field or electrical current. Experimental realisations included a CoFeB/Cu/Co spin valve on PZT in which the domain wall propagation field was doubled by a locally applied strain [38] (figures 6(c) and (d)), and a GaMnAsP ferromagnetic semiconductor microbar bonded to a PZT stressor in which the current-driven domain wall velocity was altered by the strain [39]. Both of these works used the strain-induced anisotropy to tune the spin structure of the domain walls and thereby modify their propagation by conventional means. For the next step, i.e. field and current-free domain wall motion, Van de Wiele *et al* [87] simulated a 15 nm $Co_{60}Fe_{40}$ layer in which the magnetic domain wall was pinned to a ferroelectric domain wall in an adjacent BTO substrate that was driven by a voltage. The ferroelectric domain wall is modelled as an anisotropy boundary moving with constant velocity and the magnetic domain wall is 90° and either charged or uncharged. Depending on the type of domain wall and the precise material parameters, spin wave emission and domain wall transformations were observed at high drive velocities. A subsequent experiment [88] demonstrated reproducible back-and-forth motion of a magnetic domain wall in Fe by pinning it to a BTO a–c domain boundary driven by out-of-plane electric field pulses. Based on this work, power consumption of electric field-driven magnetic domain wall motion was estimated to be several orders of magnitude smaller than for current-driven domain walls. This is very attractive for microelectronic and magnetic applications. Yet, materials processing challenges remain to incorporate multiferroic heterostructures into real device packages.

A recent experimental and computational study [89] considered the effect of stress on the magnetic structures within a multiturn counter device [15], treating it as an external effect arising unavoidably from the sensor environment or device packaging. Key to the operation of the counter is the injection of a domain wall from a large region of magnetic film (pad) into a nanowire and it is important that the magnetic field required to do this is as small as possible. However, a uniaxial strain in the plane of the film increases the injection field. The study showed that careful material preparation can reduce the effective anisotropy caused by the strain, thus keeping the domain wall injection field low even in devices that have a finite magnetostriction. Continuing with the idea of stress induced by device packaging, Masiocchi *et al* proposed selectively removing regions of a protective cap layer to induce local strain in a CoFe(B) nanowire deposited on a silicon substrate [90]. A pair of $10 \times 10\ \mu\text{m}^2$ openings in the SiN cap either side of the nanowire was shown to pin domain walls by modifying the magnetoelastic energy landscape. This design has the advantage of not requiring piezoelectric materials and holds promise for some applications.

A curved nanowire or ring may also be used to isolate individual domain walls, as shown in figure 3(b). Driving domain walls around the ring using localised strains has been proposed as a mechanism for nanoscale magnetic motors and for manipulating magnetic beads for lab-on-a-chip applications [57]. Simulations predict that in a CoFeB nanoring on a PZT disk, the average velocity of a domain wall may be up to $550\ \text{m s}^{-1}$ [91]. This is comparable to spin-torque driven magnetic domain wall motion, but with heat dissipation estimated to be 3 orders of magnitude smaller (0.2 fJ vs. 0.2 pJ per 180° domain wall circuit around the ring). Extending the simulations to highly magnetoelastic materials such as Terfenol-D showed that back-coupling of magnetization to strain should be accounted for in this case [92]. To avoid using complex electrode designs, Mathurin *et al* [93] proposed instead to use a constant bias field, a uniform stress from a piezoelectric substrate, and to tailor the static and dynamic response of a domain wall in a magnetoelastic nanowire by varying its cross section. For example, it was shown that an applied electric field may control the domain wall position in a wire element with pinched profile, and that complex profiles with two or more minima could be considered for hysteretic bistable or multistable systems. In the latter case, the variable geometry of the nanowire generates energy minima to pin domain walls. It appears that some degree of complexity is required for controlled domain wall motion—either by patterning electrodes to provide localised strains, or by patterning the magnetic strip to provide a spatially non-uniform energy landscape if a uniform strain is used. Even in the case of short strain pulses generated by a single large pair of electrodes [94], a domain wall exhibits no net displacement unless a pinning potential is provided.

The velocity of a magnetic domain wall is a figure of merit for many proposed magnetic devices, but under large driving forces the internal structure of a domain wall changes, and above a certain threshold value continuous internal precession of the domain wall takes place during its motion, with a consequent reduction in speed. A similar effect occurs in many simulations of domain wall motion in magnetic nanowires with in-plane anisotropy where the driving force is a strain gradient of piezoelectric origin [86, 91, 95]. The instability of domain walls under large strain gradients places a limit on the domain wall velocity on the order of $100\ \text{m s}^{-1}$. To overcome this limit, Fattouhi *et al* [96] tried modelling a Néel-type domain wall stabilised by iDMI in a ferromagnetic nanostrip with perpendicular anisotropy. With an in-plane strain gradient driving the domain wall along the strip as shown in figure 7, the internal angle of the domain wall changes and, crucially, depends on the strain, giving rise to a dynamic torque that prevents the onset of internal domain wall oscillations.

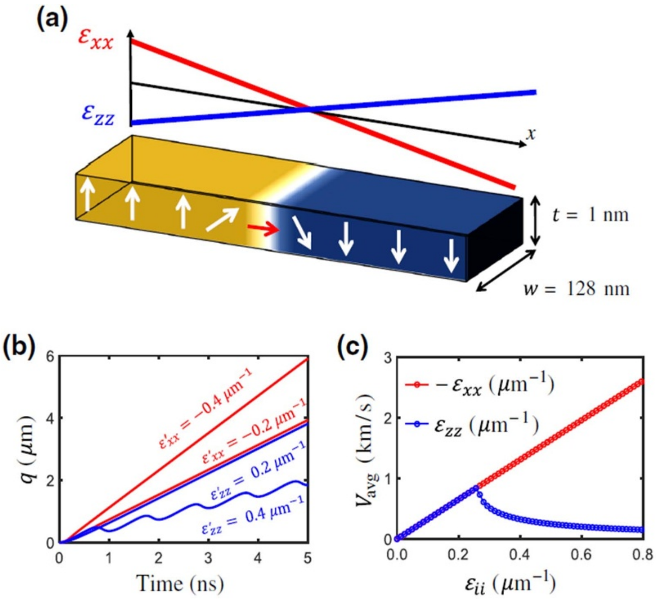

Figure 7. Strain-driven domain wall motion stabilised by iDMI. (a) Schematic representation of a Néel domain wall located at the centre of a ferromagnetic nanostrip, subject to a strain gradient. The in-plane and perpendicular strain profiles are shown by red and blue colours, respectively. (b) Domain wall position (q) versus time when driven by two different in-plane (red) and perpendicular (blue) strain gradients. (c) Average domain wall velocity versus strain slope for the in-plane (red) and perpendicular (blue) cases. Reprinted (figures) with permission from [96], Copyright (2022) by the American Physical Society.

4. Skyrmions under strain

Magnetic skyrmions were initially found at low temperatures in materials with a chiral cubic crystal structure (bulk DMI) [17, 97]. Accordingly, the first investigations of the effect of strain on skyrmions were in MnSi [98, 99], Cu_2OSeO_3 [100] and FeGe [101], e.g. Nii *et al* discovered that a uniaxial compressive strain on the order of 10^{-4} could trigger a topological phase transition in MnSi between conical and skyrmion phases [99]. The bulk crystals of these compounds host skyrmions only in small regions in the field-temperature phase space, and stabilising skyrmions over wider temperature ranges is essential for their application. Seki *et al* reported a dramatic widening of the temperature window of the skyrmion crystal phase in Cu_2OSeO_3 under <0.2% uniaxial tensile strain [100] (figures 8(a) and (b)). Meanwhile in

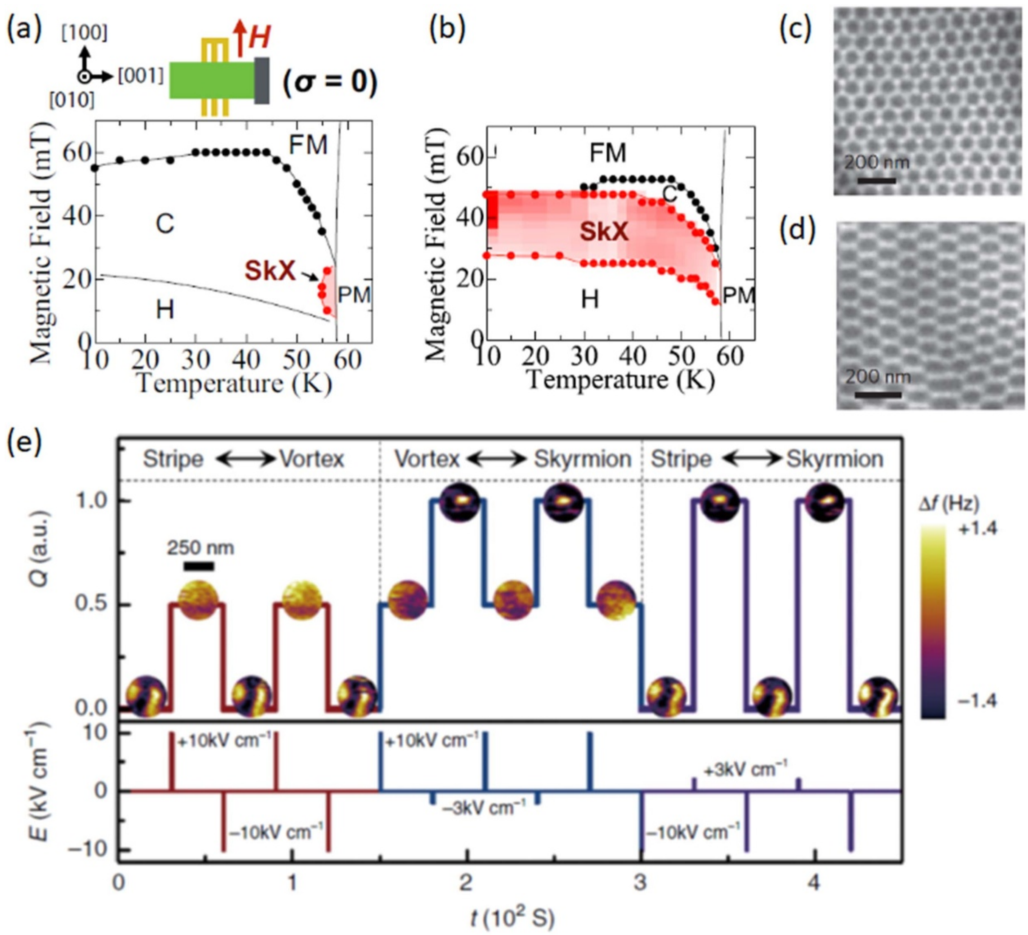

Figure 8. Skyrmions under strain. (a) Field-temperature phase diagram for unstrained Cu_2OSeO_3 obtained with the device shown. H, C, SkX, FM and PM represent helical, conical, skyrmion lattice, ferromagnetic, and paramagnetic spin states, respectively. (b) Field-temperature phase diagram for Cu_2OSeO_3 under uniaxial tensile strain σ in the [001] direction. Reprinted (figures) with permission from [100], Copyright (2017) by the American Physical Society. (c) Lorentz TEM image of a skyrmion lattice at 94 K in a FeGe thin plate that is nominally strain-free. (d) Thermal strain is applied to the FeGe in the horizontal direction. Reproduced from [101], with permission from Springer Nature. (e) Switching of topological number Q in Pt/Co/Ta multilayer dots ($Q = 1.0$, 0.5, and 0 corresponds to skyrmion, vortex and stripe domain, respectively) by applying a pulsed electric field with a duration of 1 ms. The insets contain the corresponding MFM images for the switching. Reproduced from [110].

FeGe a strain of 0.3% induced deformations of the skyrmions as well as distortions of the skyrmion crystal lattice on the order of 20%, suggesting that strain induces anisotropy in the DMI [101] (figures 8(c) and (d)). These experiments used a pressure cell (compressive) or thermal strain apparatus (tensile) to exert stress. Following the discovery of skyrmions at room temperature in metallic multilayers with interfacial DMI [102–104], strain could be applied using piezoelectric materials in a similar way to the studies of strain on magnetic domain walls in thin films. Simulations include skyrmion creation and pinning in Pd/Fe/Ir on PZT [105], triggering magnetic switching and topological transitions by strain in Pt/Co/Ta [106], and the study of strain gradients on current-driven skyrmion motion [107–109]. Yanes *et al* [107] showed that, in materials with a positive magnetostriction, a skyrmion moves towards regions of high strain, and for realistic strain gradient of order 10^{-3} μm^{-1} results in a skyrmion velocity similar to that obtained by passing a current of order 10^9 A m^{-2}.

One of the issues with current-driven skyrmions is that there is a Magnus force that moves skyrmions transverse to the current direction, the so-called skyrmion Hall effect [111]. Fattouhi *et al* [109] showed that a transverse strain gradient can be used to suppress the skyrmion Hall effect. There are a handful of experiments where magnetic multilayers with iDMI have been deposited on PMN-PT to investigate the effect of strain on skyrmions. Wang *et al* [110] patterned Pt/Co/Ta multilayer dots with sub-micron diameters to stabilise skyrmions. They discovered by applying electric field cycles from $+10$ to -10 kV cm^{-1} that stripe and vortex domains existed under compressive strain (-0.2%–0.4%) while a transformation to skyrmion state occurred under tensile strain (up to $+0.2\%$) (figure 8(e)). Without patterning a multilayer film into nanodots, skyrmions may be created but only in the presence of a bias field [112]. Control of the skyrmion phase in Pt/Co/Gd multilayers by piezoelectric strain has been shown to be promising for reservoir computing applications due to nonlinear responses in the magnetization and Hall resistivity [113]. It is likely that many potential applications of skyrmions [19, 20] may be enhanced by strain.

Another challenge with skyrmions that may be resolved in some schemes [114–116] is to stabilise them in zero magnetic field. While Wang *et al* were able, by applying a sequence of electric fields, to generate a skyrmion state in Pt/Co/Ta multilayer dots deposited on PMN-PT in zero magnetic field [110] (figure 8(e)), a recent work predicts that compressive strain stabilises zero field skyrmions in a Fe_3GeTe_2/germanene van der Waals heterostructure [117]. Here the strain arises from the buckled substrate and not from a piezoelectric. Zero field antiferromagnetic skyrmions have been stabilised at room temperature in a synthetic antiferromagnet [118] and predicted in a non-synthetic system [119]. Skyrmions in ferrimagnetic systems have also been observed [120], including in zero field [121]. The strain effect on skyrmions in antiferromagnetic and ferrimagnetic systems has, however, been little investigated so far, e.g. it was considered by Roy *et al* in their study of skyrmion dynamics in a synthetic ferrimagnet [122], and discussed by Khoshlahni *et al* in the context of SAWs [123].

5. Domain wall and skyrmion manipulation by SAWs

SAWs are elastic waves propagating on the surface of a solid and in the 1960s it became possible to efficiently excite and detect them at microwave frequencies by using interdigitated transducers (IDTs) on top of piezoelectric substrates [124]. Soon afterwards, the interaction of SAWs and thin magnetic films began to be investigated, but the potential for SAWs to drive magnetization dynamics such as ferromagnetic resonance was only established relatively recently [125, 126]. Reports of SAW-assisted magnetization switching in thin GaMnAsP layers [127, 128] have led researchers to consider the dynamic strain profiles of SAWs as means to manipulate domain walls and skyrmions in thin films.

The micromagnetic simulations by Dean *et al* [129] acted as catalyst for experiments investigating the interaction of SAWs and domain walls. They showed that a pair of IDTs could generate domain wall pinning sites in a magnetostrictive nanowire by forming a standing strain wave along its length (figure 9(a)). The antinodes of the standing SAW are the pinning sites because the strain gradient which drives the domain walls is maximum at the nodes and zero at the antinodes. Although the antinodes alternate between compressive and tensile stress, if a domain wall travels towards an antinode in the first half of an oscillation cycle, it will experience smaller strain gradient in the second half and so on, thus producing a net displacement towards the antinode. Shifting the frequency of one IDT, the standing wave drifted and the domain walls could be transported at the drift velocity up to 50 m s^{-1} (figure 9(b)). In experiments, Edrington *et al* showed that standing SAWs effectively drive domain wall motion from the creep regime to the flow regime in Co/Pt multilayers [130] (figure 9(c)). Adhikari *et al* explored how standing SAWs enhance domain wall motion in the creep regime and increase the likelihood of domain wall depinning in Co/Pt multilayer wires [131, 132] (figure 9(d)). In these experiments and others [133–135] the SAW assists the magnetic field or spin torque switching of magnetization. Shuai *et al* showed that heating from rf power dissipation at the IDTs plays a role [136] (figure 9(e,f)). Interestingly, a travelling SAW had little effect on the field-driven domain wall creep over and above the heating effect, while a standing SAW of equivalent power did. To understand the travelling SAW effect on domain wall dynamics, micromagnetic simulations were performed for films with different levels of disorder, modelled as anisotropy distribution within grains [137]. It was found that for low levels of disorder, the domain wall velocity decreases with increasing SAW frequency due to SAW-induced energy dissipation via spin rotation. However, for larger levels of disorder the spin rotation enhances the domain wall depinning from positions of high anisotropy, and improves the velocity. This agrees with the semi-analytic model in [129], in that the primary role of the SAW is to drive oscillations of the internal domain wall magnetization; but it also shows that these oscillations can help or hinder domain wall motion depending on the disorder. The heating effect of SAWs may thus be the main driver of domain wall depinning or creep, depending on the level of disorder in the material.

On the interaction of skyrmions and SAWs, there have been some simulation and analytical studies. Nepal *et al* [141] showed that, using Thiele's approach, the force that pushes the skyrmion is proportional to the strain gradient, similar to the case of domain walls [129]. The number of skyrmions created in a magnetic multilayer with iDMI was found to increase monotonically with increasing SAW amplitude [138] (figure 10(a-c)). Experimentally a similar effect was noted in Pt/Co/Ir multilayers [142] and, further, it was shown that bubble domains nucleated preferentially at antinodes where the (dynamic) variation of anisotropy was greatest [42] (figure 10(d,e)). Recent works have explored different SAW geometries and SAW-assisted skyrmion motion, e.g. using two orthogonal standing SAWs for precise positioning of skyrmions in 2D [143], current-driven skyrmions with the skyrmion Hall effect suppressed by a standing SAW [139, 144], skyrmions driven by the shear horizontal mode of a SAW [145], and travelling SAW-driven skyrmion motion with orthogonal standing SAW [140] (figure 10(f-h)). The advantage of SAWs is that several skyrmions may be remotely manipulated, and the SAW geometry can be arranged to exploit the 2D nature of skyrmions. The interaction between SAWs and other topological spin structures are being investigated [123, 146].

6. Outlook

We conclude this review by looking through the lens of applications. For magnetic memory such as MRAM, 180° reversal of magnetisation at ultralow power is a key technological goal, and, recently, magnetoelectric switching of a CoFe/Cu/CoFe spin valve on La-BFO was shown to operate at or below 200 mV, approaching the desired attojoule switching regime

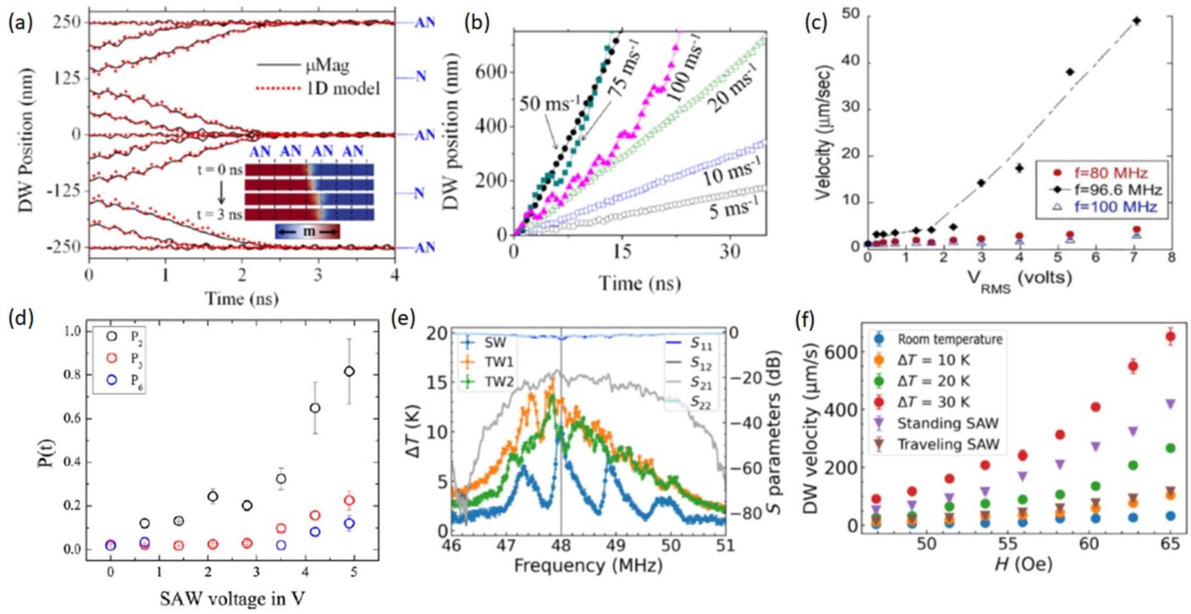

Figure 9. SAW effect on domain walls. (a) Results of micromagnetic simulations showing how the position of a domain wall evolves when it is placed at variable distances from the central antinode of a standing stress/strain wave (SAW amplitude 30 MPa, $\lambda = 500$ nm, $f = 4.23$ GHz). The dotted lines indicate the results of equivalent simulations performed using a 1D semi-analytical model. The inset shows the dynamics of a domain wall initially located 150 nm from the standing wave's central antinode. (b) Dynamics of domain walls subjected to standing waves created in moving frames of reference with $v = 5$–100 m s^{-1}. Reprinted from [129], with the permission of AIP Publishing. (c) Domain wall velocity in a Co/Pt multilayer as a function of applied voltage, at three different standing SAW frequencies. Reprinted from [130], with the permission of AIP Publishing. (d) Depinning probability P(t) of a domain wall in Co/Pt as a function of SAW voltage for three representative pinning sites. Reproduced from [132]. © IOP Publishing Ltd All rights reserved. (e) Temperature changes ΔT of a Pt thin film thermometer within a SAW beam path as a function of source frequency from 46 to 51 MHz with rf power of 21 dBm. SW, TW1 and TW2 denote standing SAWs, traveling SAWs launched from IDT1 of a pair of interdigitated transducers, and traveling SAWs launched from IDT2, respectively. Reproduced from [136]. CC BY 4.0. (f) DW velocity as a function of applied magnetic field H, measured at different temperatures from room temperature up to $\Delta T = 30$ K without SAWs (circles) and in the presence of standing SAWs and travelling SAWs at a centre frequency of 48 MHz and rf power of 21 dBm without additional heating (triangles). Reproduced from [136]. CC BY 4.0.

[147]. Lanthanum substitution and thickness scaling in BFO has helped to scale the switching energy density to 10 μJ cm^{-2} and indicates a route to achieve aJ nonvolatile memories [148].

Going beyond a 180° macrospin switching in a memory cell, however, magnetic domain walls promise sophisticated racetrack memory, logic and unconventional computing schemes, as well as various options for sensing, and strain coupling to a piezoelectric would serve to enhance the functionality of these devices. Of the piezoelectric substrates, BTO is interesting due to its structural phase transition close to 0 °C, different cuts leading to different angles between ferroelectric polarisation in neighbouring domains [66], and the various domain wall spin structures that can coexist within a thin magnetic film [68]. The possibility to choose different domain wall types within one device, or to tune the domain wall width by strain or field, offers new opportunities in device design. In thin films with PMA, 90° switching in Cu/Ni on BTO [77] is potentially of interest for a magnetoresistive sensor, as is the change in direction of stripe domains in Py [70] or multilayer with interface anisotropy. The manipulation of PMA and iDMI by strain could enable tuning of domain wall spin structures and their chirality but it is still an open question as to whether these effects are large enough to be useful. Anisotropic iDMI has been generated in magnetic films on D2d substrates to form anti-skyrmions but to transform between topological states by piezoelectric strain has so far only been demonstrated in simulations [106].

Isolating magnetic domain walls in a nanostrip has proven to be a useful way to study individual domain walls and their response to strain. If applied via specially designed electrical contacts, strain pulses or gradients could replace spin-orbit torque as a domain wall driving mechanism and have the benefit of lower energy dissipation. Driving domain walls around a nanoring (Ni/PMN-PT) all electrically is a good example of this [57]. Replacing lead-based piezoelectrics is desirable from an environmental perspective, and it has been shown that driving a ferroelectric–ferromagnet domain wall pair by electric field works in principle [87, 88], but challenges remain to incorporate this scheme into a device. An alternative solution is to use less complex device designs, e.g. to remove the piezoelectric and use instead a patterned capping layer, or to use an engineered shape of the thin magnetic structure to break symmetry, or even to consider 3D magnetic structures.

Finally, static and dynamic strain provide additional degrees of freedom to control skyrmion motion, impacting on design of skyrmion-based memories, logic and neuromorphic

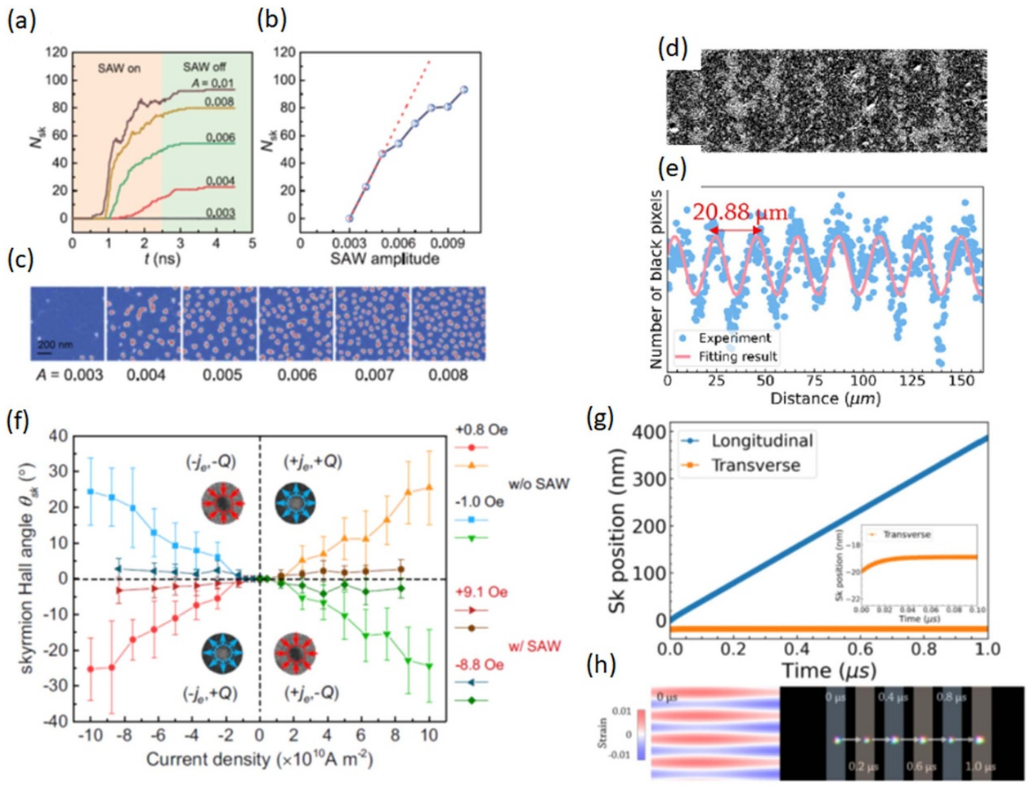

Figure 10. SAW effect on skyrmions. (a) Micromagnetic simulations of the number of created skyrmions in a Co/Pt thin film with SAWs applied for 2.5 ns. The different datasets are for different SAW amplitudes. Reproduced from [138]. (b) Number of skyrmions with respect to the SAW amplitude at $t = 4.5$ ns Reproduced from [138]. (c) Illustrations of skyrmions created with different SAW amplitudes corresponding to (b) at $t = 4.5$ ns. The film size is 1024×1024 nm^2. Reproduced from [138]. (d) Domain patterns in Pt/Co/Ir thin film with both magnetic field (3.6 mT) and 93.35 MHz standing SAW at 22.5 dBm. Reproduced from [42]. (e) The number of black pixels in (d) and its sinusoidal fitting, indicating a wavelength of 20.88 μm, similar to the half-wavelength of the standing SAW ($\sim$21 μm). Reproduced from [42]. (f) Phase diagram of skyrmion Hall angle θ_{sk} as a function of current density measured with and without SAWs for skyrmions in a Co/Pd/Co/Pd/Co/Pt multilayer with topological charge $Q = +1$ and $Q = -1$. The insets show the magnetic configurations of the skyrmions with opposite topological charge. Reproduced from [139]. (g) Translation of skyrmion in Co/Pt bilayer in x and y directions, driven by combined travelling and standing SAWs (simulation). The inset graph shows the skyrmion motion in the y direction during the first 0.1 μs. (h) Left hand side shows the spatial strain profile of orthogonal SAWs at 0 μs. Right hand side shows snapshots of the skyrmion motion from 0 to 1.0 μs. The shaded areas indicate the skyrmion positions at the corresponding time. The arrows indicate the direction of skyrmion motion. After [140].

computing devices. SAWs permit remote and reconfigurable control of domain walls and skyrmions and offer a route to scaling down of power requirements due to their ability to propagate over cm scale with minimal amplitude decay. This potentially allows a single pair of SAW transducers to simultaneously control many spin textures.

Data availability statement

No new data were created or analysed in this study.

Acknowledgment

The author gratefully acknowledges funding from the European Union's Horizon 2020 research and innovation programme under Marie Sklodowska-Curie Grant Agreement No. 860060 'Magnetism and the effect of Electric Field' (MagnEFi).

ORCID iD

Thomas A Moore https://orcid.org/0000-0001-6443-2556

References

[1] Hubert A and Schäfer R 1998 *Magnetic Domains: The Analysis of Magnetic Microstructures* (Springer)
[2] Schryer N L and Walker L R 1974 The motion of 180° domain walls in uniform dc magnetic fields *J. Appl. Phys.* **45** 5406
[3] Malozemoff A P and Slonczewski J C 1979 *Magnetic Domain Walls in Bubble Materials* (Academic)
[4] Berger L 1984 Exchange interaction between ferromagnetic domain wall and electric current in very thin metallic films *J. Appl. Phys.* **55** 1954
[5] Allwood D A, Xiong G, Faulkner C C, Atkinson D, Petit D and Cowburn R P 2005 Magnetic domain-wall logic *Science* **309** 1688
[6] Luo Z, Hrabec A, Dao T P, Sala G, Finizio S, Feng J, Mayr S, Raabe J, Gambardella P and Heyderman L J 2020

Current-driven magnetic domain-wall logic *Nature* **579** 214

[7] Parkin S S P, Hayashi M and Thomas L 2008 Magnetic domain-wall racetrack memory *Science* **320** 190

[8] Fukami S *et al* 2009 Low-current perpendicular domain wall motion cell for scalable high-speed MRAM *Symp. on VLSI Technology* (*Kyoto, Japan*) p 230

[9] Thiaville A and Nakatani Y 2006 *Spin Dynamics in Confined Magnetic Structures* vol III, ed B Hillebrands and K Ounadjela (Springer)

[10] Kläui M 2008 Head-to-head domain walls in magnetic nanostructures *J. Phys.: Condens. Matter* **20** 313001

[11] Yue K, Liu Y, Lake R K and Parker A C 2019 A brain-plausible neuromorphic on-the-fly learning system implemented with magnetic domain wall analog memristors *Sci. Adv.* **5** eaau8170

[12] Siddiqui S A, Dutta S, Tang A, Liu L, Ross C A and Baldo M A 2020 Magnetic domain wall based synaptic and activation function generator for neuromorphic accelerators *Nano Lett.* **20** 1033

[13] Cui C, Akinola O G, Hassan N, Bennett C H, Marinella M J, Friedman J S and Incorvia J A C 2020 Maximised lateral inhibition in paired magnetic domain wall racetracks for neuromorphic computing *Nanotechnology* **31** 294001

[14] Ababei R V, Ellis M O A, Vidamour I T, Devadasan D S, Allwood D A, Vasilaki E and Hayward T J 2021 Neuromorphic computation with a single magnetic domain wall *Sci. Rep.* **11** 15587

[15] Diegel M, Mattheis R and Halder E 2007 Multiturn counter using movement and storage of 180° domain walls *Sens. Lett.* **5** 118

[16] Thiaville A, Rohart S, Jué E, Cros V and Fert A 2012 Dynamics of Dzyaloshinskii domain walls in ultrathin magnetic films *EPL* **100** 57002

[17] Yu X Z, Onose Y, Kanazawa N, Park J H, Han J H, Matsui Y, Nagaosa N and Tokura Y 2010 Real-space observation of a two-dimensional skyrmion crystal *Nature* **465** 901

[18] Heinze S, von Bergmann K, Menzel M, Brede J, Kubetzka A, Wiesendanger R, Bihlmayer G and Blügel S 2011 Spontaneous atomic-scale magnetic skyrmion lattice in two dimensions *Nat. Phys.* **7** 713

[19] Li S, Kang W, Zhang X, Nie T, Zhou Y, Wang K L and Zhao W 2021 Magnetic skyrmions for unconventional computing *Mater. Horiz.* **8** 854

[20] Luo S and You L 2021 Skyrmion devices for memory and logic applications *APL Mater.* **9** 050901

[21] Huang Y, Kang W, Zhang X, Zhou Y and Zhao W 2017 Magnetic skyrmion-based synaptic devices *Nanotechnology* **28** 08LT02

[22] Soumyanarayanan A, Reyren N, Fert A and Panagopoulos C 2016 Emergent phenomena induced by spin-orbit coupling at surfaces and interfaces *Nature* **539** 509

[23] Kumar D, Jin T, Sbiaa R, Kläui M, Bedanta S, Fukami S, Ravelosona D, Yang S-H, Liu X and Piramanayagam S N 2022 Domain Wall Memory: Physics, Materials, and Devices *Phys. Rep.* **958** 1

[24] Nagaosa N and Tokura Y 2013 Topological properties and dynamics of magnetic skyrmions *Nat. Nanotechnol.* **8** 899

[25] Wiesendanger R 2016 Nanoscale magnetic skyrmions in metallic films and multilayers: a new twist for spintronics *Nat. Rev. Mater.* **1** 16044

[26] Kang W, Huang Y, Zhang X, Zhou Y and Zhao W 2016 Skyrmion-electronics: an overview and outlook *Proc. IEEE* **104** 2040

[27] Fert A, Reyren N and Cros V 2017 Magnetic skyrmions: advances in physics and potential applications *Nat. Rev. Mater.* **2** 17031

[28] Jiang W, Chen G, Liu K, Zang J, te Velthuis S G E and Hoffmann A 2017 Skyrmions in magnetic multilayers *Phys. Rep.* **704** 1

[29] Everschor-Sitte K, Masell J, Reeve R M and Kläui M 2018 Perspective: magnetic skyrmions—overview of recent progress in an active research field *J. Appl. Phys.* **124** 240901

[30] Zhang X, Zhou Y, Song K M, Park T-E, Xia J, Ezawa M, Liu X, Zhao W, Zhao G and Woo S 2020 Skyrmion-electronics: writing, deleting, reading and processing magnetic skyrmions toward spintronic applications *J. Phys.: Condens. Matter* **32** 143001

[31] Weisheit M, Fähler S, Marty A, Souche Y, Poinsignon C and Givord D 2007 Electric field-induced modification of magnetism in thin-film ferromagnets *Science* **315** 349

[32] Maruyama T *et al* 2009 Large voltage-induced magnetic anisotropy change in a few atomic layers of iron *Nat. Nanotechnol.* **4** 158

[33] Wang K L, Alzate J G and Amiri P K 2013 Low-power non-volatile spintronic memory: STT-RAM and beyond *J. Phys. D: Appl. Phys.* **46** 074003

[34] Chiba D, Fukami S, Shimamura K, Ishiwata N, Kobayashi K and Ono T 2011 Electrical control of the ferromagnetic phase transition in cobalt at room temperature *Nat. Mater.* **10** 853

[35] Schellekens A J, van den Brink A, Franken J H, Swagten H J M and Koopmans B 2012 Electric-field control of domain wall motion in perpendicularly magnetized materials *Nat. Commun.* **3** 847

[36] Huang Z *et al* 2013 Ferroelectric control of magnetic domains in ultra-thin cobalt layers *Appl. Phys. Lett.* **103** 222902

[37] Bauer U, Yao L, Tan A J, Agrawal P, Emori S, Tuller H L, van Dijken S and Beach G S D 2014 Magneto-ionic control of interfacial magnetism *Nat. Mater.* **14** 174

[38] Lei N *et al* 2013 Strain-controlled magnetic domain wall propagation in hybrid piezoelectric/ferromagnetic structures *Nat. Commun.* **4** 1378

[39] De Ranieri E *et al* 2013 Piezoelectric control of the mobility of a domain wall driven by adiabatic and non-adiabatic torques *Nat. Mater.* **12** 808

[40] Shepley P M, Rushforth A W, Wang M, Burnell G and Moore T A 2015 Modification of perpendicular magnetic anisotropy and domain wall velocity in Pt/Co/Pt by voltage-induced strain *Sci. Rep.* **5** 7921

[41] Jaeger J V *et al* 2013 Picosecond inverse magnetostriction in galfenol thin films *Appl. Phys. Lett.* **103** 032409

[42] Shuai J, Ali M, Lopez-Diaz L, Cunningham J E and Moore T A 2022 Local anisotropy control of Pt/Co/Ir thin film with perpendicular magnetic anisotropy by surface acoustic waves *Appl. Phys. Lett.* **120** 252402

[43] Bandyopadhyay S, Atulasimha J and Barman A 2021 Magnetic straintronics: manipulating the magnetization of magnetostrictive nanomagnets with strain for energy-efficient applications *Appl. Phys. Rev.* **8** 041323

[44] Eerenstein W, Wiora M, Prieto J L, Scott J F and Mathur N D 2007 Giant sharp and persistent converse magnetoelectric effects in multiferroic epitaxial heterostructures *Nat. Mater.* **6** 348

[45] Eerenstein W, Mathur N D and Scott J F 2006 Multiferroic and magnetoelectric materials *Nature* **442** 759

[46] Ramesh R and Spaldin N A 2007 Multiferroics: progress and prospects in thin films *Nat. Mater.* **6** 21

[47] Chu Y-H *et al* 2008 Electric-field control of local ferromagnetism using a magnetoelectric multiferroic *Nat. Mater.* **7** 478

[48] Heron J T, Trassin M, Ashraf K, Gajek M, He Q, Yang S Y, Nikonov D E, Chu Y-H, Salahuddin S and Ramesh R 2011 Electric-field-induced magnetization reversal in a

ferromagnet-multiferroic heterostructure *Phys. Rev. Lett.* **107** 217202
[49] Heron J T *et al* 2014 Deterministic switching of ferromagnetism at room temperature using an electric field *Nature* **516** 370
[50] Trassin M, Clarkson J D, Bowden S R, Liu J, Heron J T, Paull R J, Arenholz E, Pierce D T and Unguris J 2013 Interfacial coupling in multiferroic/ferromagnet heterostructures *Phys. Rev.* B **87** 134426
[51] De Luca G, Schoenherr P, Mendil J, Meier D, Fiebig M and Trassin M 2018 Domain-pattern transfer across an artificial magnetoelectric interface *Phys. Rev. Appl.* **10** 054030
[52] Cui J, Liang C-Y, Paisley E A, Sepulveda A, Ihlefeld J F, Carman G P and Lynch C S 2015 Generation of localized strain in a thin film piezoelectric to control individual magnetoelectric heterostructures *Appl. Phys. Lett.* **107** 092903
[53] Chopdekar R V, Heidler J, Piamonteze C, Takamura Y, Scholl A, Rusponi S, Brune H, Heyderman L J and Nolting F 2013 Strain-dependent magnetic configurations in manganite-titanate heterostructures probed with soft x-ray techniques *Eur. Phys. J.* B **86** 241
[54] Finizio S *et al* 2014 Magnetic anisotropy engineering in thin film Ni nanostructures by magnetoelastic coupling *Phys. Rev. Appl.* **1** 021001
[55] Chung T-K, Carman G P and Mohanchandra K P 2008 Reversible magnetic domain-wall motion under an electric field in a magnetoelectric thin film *Appl. Phys. Lett.* **92** 112509
[56] Chung T K, Keller S and Carman G P 2009 Electric-field-induced reversible magnetic single-domain evolution in a magnetoelectric thin film *Appl. Phys. Lett.* **94** 132501
[57] Sohn H *et al* 2015 Electrically driven magnetic domain wall rotation in multiferroic heterostructures to manipulate suspended on-chip magnetic particles *ACS Nano* **9** 4814
[58] Biswas A K, Ahmad H, Atulasimha J and Bandyopadhyay S 2017 Experimental demonstration of complete 180° reversal of magnetization in isolated Co nanomagnets on a PMN-PT substrate with voltage generated strain *Nano Lett.* **17** 3478
[59] Lahtinen T H E, Shirahata Y, Tao L, Franke K J A, Venkataiah G, Taniyama T and van Dijken S 2012 Alternating domains with uniaxial and biaxial magnetic anisotropy in epitaxial Fe films on $BaTiO_3$ *Appl. Phys. Lett.* **101** 262405
[60] Lahtinen T H E, Franke K J A and van Dijken S 2012 Electric-field control of magnetic domain wall motion and local magnetization reversal *Sci. Rep.* **2** 258
[61] Lahtinen T H E and van Dijken S 2013 Temperature control of local magnetic anisotropy in multiferroic CoFe/$BaTiO_3$ *Appl. Phys. Lett.* **102** 112406
[62] Streubel R, Köhler D, Schäfer R and Eng L M 2013 Strain-mediated elastic coupling in magnetoelectric nickel/barium-titanate heterostructures *Phys. Rev.* B **87** 054410
[63] Franke K J A, Lahtinen T H E and van Dijken S 2012 Field tuning of ferromagnetic domain walls on elastically coupled ferroelectric domain boundaries *Phys. Rev.* B **85** 094423
[64] Casiraghi A, Domínguez T R, Rößler S, Franke K J A, Gonzalez D L, Hämäläinen S J, Frömter R, Oepen H P and van Dijken S 2015 Influence of elastically pinned magnetic domain walls on magnetization reversal in multiferroic heterostructures *Phys. Rev.* B **92** 054406
[65] Gonzalez D L, Casiraghi A, Kronast F, Franke K J A and van Dijken S 2017 Influence of magnetic field and ferromagnetic film thickness on domain pattern transfer in multiferroic heterostructures *J. Magn. Magn. Mater.* **441** 404
[66] Franke K J A, Ophus C, Schmid A K and Marrows C H 2023 60° and 120° domain walls in epitaxial $BaTiO_3$(111)/Co multiferroic heterostructures *Phys. Rev.* B **107** L140407
[67] Franke K J A, Ophus C, Schmid A K and Marrows C H 2023 Competition between exchange and magnetostatic energies in domain pattern transfer from $BaTiO_3$(111) to a Ni thin film *Phys. Rev. Mater.* **7** 034403
[68] Hunt R G, Franke K J A, Shepley P M and Moore T A 2023 Strain-coupled domains in $BaTiO_3$(111)-CoFeB heterostructures *Phys. Rev.* B **107** 014409
[69] Hunt R G, Franke K J A, Keatley P S, Shepley P M, Rogers M and Moore T A 2023 Temperature dependence of magnetic anisotropy and domain wall tuning in $BaTiO_3$(111)/CoFeB multiferroics *APL Mater.* **11** 071112
[70] Fackler S W, Donahue M J, Gao T, Nero P N A, Cheong S-W, Cumings J and Takeuchi I 2014 Local control of magnetic anisotropy in transcritical permalloy thin films using ferroelectric $BaTiO_3$ domains *Appl. Phys. Lett.* **105** 212905
[71] Franke K J A, Ophus C, Schmid A K and Marrows C H 2021 Switching between magnetic Bloch and Néel domain walls with anisotropy modulations *Phys. Rev. Lett.* **127** 127203
[72] Nakajima N, Koide T, Shidara T, Miyauchi H, Fukutani H, Fujimori A, Iio K, Katayama T, Nyvlt M and Suzuki Y 1998 Perpendicular magnetic anisotropy caused by interfacial hybridization via enhanced orbital moment in Co/Pt multilayers: magnetic circular dichroism study *Phys. Rev. Lett.* **81** 5229
[73] Visokay M R and Sinclair R 1995 Direct formation of ordered CoPt and FePt compound thin films by sputtering *Appl. Phys. Lett.* **66** 1692
[74] Saito N, Fujiwara H and Sugita Y 1964 A new type of magnetic domain structure in negative magnetostriction Ni-Fe films *J. Phys. Soc. Japan* **19** 1116
[75] Mimura Y, Inamura N and Kobayashi T 1976 Magnetic properties and curie point writing in amorphous metallic films *IEEE Trans. Magn.* **12** 779
[76] Ghidini M *et al* 2015 Perpendicular local magnetization under voltage control in Ni films on ferroelectric $BaTiO_3$ substrates *Adv. Mater.* **27** 1460
[77] Shirahata Y, Shiina R, Gonzalez D L, Franke K J A, Wada E, Itoh M, Pertsev N A, van Dijken S and Taniyama T 2015 Electric-field switching of perpendicularly magnetized multilayers *npg Asia Mater.* **7** e198
[78] Gonzalez D L, Shirahata Y, Van de Wiele B, Franke K J A, Casiraghi A, Taniyama T and van Dijken S 2017 Electric-field-driven domain wall dynamics in perpendicularly magnetized multilayers *AIP Adv.* **7** 035119
[79] Rousseau O, Weil R, Rohart S and Mougin A 2016 Strain-induced magnetic domain wall control by voltage in hybrid piezoelectric $BaTiO_3$ ferrimagnetic TbFe structures *Sci. Rep.* **6** 23038
[80] Feng C *et al* 2016 Nonvolatile modulation of electronic structure and correlative magnetism of $L1_0$-FePt films using significant strain induced by shape memory substrates *Sci. Rep.* **6** 20199
[81] Gopman D B, Dennis C L, Chen P J, Iunin Y L, Finkel P, Staruch M and Shull R D 2016 Strain-assisted magnetization reversal in Co/Ni multilayers with perpendicular magnetic anisotropy *Sci. Rep.* **6** 27774
[82] Chen G, N'Diaye A T, Kang S P, Kwon H Y, Won C, Wu Y, Qiu Z Q and Schmid A K 2015 Unlocking Bloch-type chirality in ultrathin magnets through uniaxial strain *Nat. Commun.* **6** 6598
[83] Gusev N S, Sadovnikov A V, Nikitov S A, Sapozhnikov M V and Udalov O G 2020 Manipulation of the

Dzyaloshinskii-Moriya interaction in Co/Pt multilayers with strain *Phys. Rev. Lett.* **124** 157202

[84] Sapozhnikov M V, Gorev R V, Skorokhodov E V, Gusev N S, Sadovnikov A V and Udalov O G 2022 Zigzag domains caused by strain-induced anisotropy of the Dzyaloshinskii-Moriya interaction *Phys. Rev.* B **105** 024405

[85] Dean J, Bryan M T, Schrefl T and Allwood D A 2011 Stress-based control of magnetic nanowire domain walls in artificial multiferroic systems *J. Appl. Phys.* **109** 023915

[86] Bryan M T, Dean J and Allwood D A 2012 Dynamics of stress-induced domain wall motion *Phys. Rev.* B **85** 144411

[87] Van de Wiele B, Laurson L, Franke K J A and van Dijken S 2014 Electric field driven magnetic domain wall motion in ferromagnetic-ferroelectric heterostructures *Appl. Phys. Lett.* **104** 012401

[88] Franke K J A, Van de Wiele B, Shirahata Y, Hamalainen S J, Taniyama T and van Dijken S 2015 Reversible electric-field-driven magnetic domain-wall motion *Phys. Rev.* X **5** 011010

[89] Masiocchi G, Fattouhi M, Kehlberger A, Lopez-Diaz L, Syskaki M-A and Kläui M 2021 Strain-controlled domain wall injection into nanowires for sensor applications *J. Appl. Phys.* **130** 183903

[90] Masiocchi G, Fattouhi M, Spetzler E, Syskaki M-A, Lehndorff R, Martinez E, McCord J, Lopez Diaz L, Kehlberger A and Kläui M 2023 Generation of imprinted strain gradients for spintronics *Appl. Phys. Lett.* **123** 022404

[91] Hu J-M *et al* 2016 Fast magnetic domain-wall motion in a ring-shaped nanowire driven by a voltage *Nano Lett.* **16** 2341

[92] Xiao Z, Lo Conte R, Chen C, Liang C-Y, Sepulveda A, Bokor J, Carman G P and Candler R N 2018 Bi-directional coupling in strain-mediated multiferroic heterostructures with magnetic domains and domain wall motion *Sci. Rep.* **8** 5207

[93] Mathurin T, Giordano S, Dusch Y, Tiercelin N, Pernod P and Preobrazhensky V 2017 Domain-wall dynamics in magnetoelastic nanostripes *Phys. Rev.* B **95** 140405(R)

[94] Rushforth A W, Rowan-Robinson R and Zemen J 2020 Deterministic magnetic domain wall motion induced by pulsed anisotropy energy *J. Phys. D: Appl. Phys.* **53** 164001

[95] Yu G, Shi S, Peng R, Guo R, Qiu Y, Wu G, Li Y, Zhu M and Zhou H 2022 Strain-driven magnetic domain wall dynamics controlled by voltage in multiferroic heterostructures *J. Magn. Magn. Mater.* **552** 169229

[96] Fattouhi M, Garcia-Sanchez F, Yanes R, Raposo V, Martinez E and Lopez-Diaz L 2022 Absence of Walker breakdown in the dynamics of chiral Néel domain walls driven by in-plane strain gradients *Phys. Rev. Appl.* **18** 044023

[97] Mühlbauer S, Binz B, Jonietz F, Pfleiderer C, Rosch A, Neubauer A, Georgii R and Böni P 2009 Skyrmion lattice in a chiral magnet *Science* **323** 915

[98] Chacon A, Bauer A, Adams T, Rucker F, Brandl G, Georgii R, Garst M and Pfleiderer C 2015 Uniaxial pressure dependence of magnetic order in MnSi *Phys. Rev. Lett.* **115** 267202

[99] Nii Y, Nakajima T, Kikkawa A, Yamasaki Y, Ohishi K, Suzuki J, Taguchi Y, Arima T, Tokura Y and Iwasa Y 2015 Uniaxial stress control of skyrmion phase *Nat. Commun.* **6** 8539

[100] Seki S, Okamura Y, Shibata K, Takagi R, Khanh N D, Kagawa F, Arima T and Tokura Y 2017 Stabilization of magnetic skyrmions by uniaxial tensile strain *Phys. Rev.* B **96** 220404R

[101] Shibata K *et al* 2015 Large anisotropic deformation of skyrmion in strained crystal *Nat. Nanotechnol.* **10** 589

[102] Jiang W *et al* 2015 Blowing magnetic skyrmion bubbles *Science* **349** 283

[103] Moreau-Luchaire C *et al* 2016 Additive interfacial chiral interaction in multilayers for stabilization of small individual skyrmions at room temperature *Nat. Nanotechnol.* **11** 444

[104] Woo S *et al* 2016 Observation of room-temperature magnetic skyrmions and their current-driven dynamics in ultrathin metallic ferromagnets *Nat. Mater.* **15** 501

[105] Li Z, Zhang Y, Huang Y, Wang C, Zhang X, Liu Y, Zhou Y, Kang W, Koli S C and Lei N 2018 Strain-controlled skyrmion creation and propagation in ferroelectric/ferromagnetic hybrid wires *J. Magn. Magn. Mater.* **455** 19

[106] Mehmood N, Song X, Tian G, Hou Z, Chen D, Fan Z, Qin M, Gao X and Liu J-M 2020 Strain-mediated electric manipulation of magnetic skyrmion and other topological states in geometric confined nanodiscs *J. Phys. D: Appl. Phys.* **53** 014007

[107] Yanes R, Garcia-Sanchez F, Luis R F, Martinez E, Raposo V, Torres L and Lopez-Diaz L 2019 Skyrmion motion induced by voltage-controlled in-plane strain gradients *Appl. Phys. Lett.* **115** 132401

[108] Liu Y, Huo X, Xuan S and Yan H 2019 Manipulating movement of skyrmion by strain gradient in a nanotrack *J. Magn. Magn. Mater.* **492** 165659

[109] Fattouhi M, Garcia-Sanchez F, Yanes R, Raposo V, Martinez E and Lopez-Diaz L 2021 Electric field control of the skyrmion Hall effect in piezoelectric-magnetic devices *Phys. Rev. Appl.* **1** 044035

[110] Wang Y *et al* 2020 Electric-field-driven non-volatile multi-state switching of individual skyrmions in a multiferroic heterostructure *Nat. Commun.* **11** 3577

[111] Jiang W *et al* 2017 Direct observation of the skyrmion Hall effect *Nat. Phys.* **13** 162

[112] Ba Y *et al* 2021 Electric-field control of skyrmions in multiferroic heterostructure via magnetoelectric coupling *Nat. Commun.* **12** 322

[113] Sun Y *et al* 2023 Experimental demonstration of a skyrmion-enhanced strain-mediated physical reservoir computing system *Nat. Commun.* **14** 3434

[114] Gallagher J C, Meng K Y, Brangham J T, Wang H L, Esser B D, McComb D W and Yang F Y 2017 Robust zero-field skyrmion formation in FeGe epitaxial thin films *Phys. Rev. Lett.* **118** 027201

[115] Meyer S, Perini M, von Malottki S, Kubetzka A, Wiesendanger R, von Bergmann K and Heinze S 2019 Isolated zero field sub-10 nm skyrmions in ultrathin Co films *Nat. Commun.* **10** 3823

[116] Zhou Y, Mansell R and van Dijken S 2021 Voltage control of skyrmions: creation, annihilation, and zero-magnetic field stabilization *Appl. Phys. Lett.* **118** 172409

[117] Li D, Haldar S and Heinze S 2022 Strain-driven zero-field near-10 nm skyrmions in two-dimensional van der Waals heterostructures *Nano Lett.* **22** 7706

[118] Legrand W, Maccariello D, Ajejas F, Collin S, Vecchiola A, Bouzehouane K, Reyren N, Cros V and Fert A 2020 Room-temperature stabilization of antiferromagnetic skyrmions in synthetic antiferromagnets *Nat. Mater.* **19** 34

[119] Aldarawsheh A, Fernandes I L, Brinker S, Sallermann M, Abusaa M, Blügel S and Lounis S 2022 Emergence of zero-field non-synthetic single and interchained antiferromagnetic skyrmions in thin films *Nat. Commun.* **13** 7369

[120] Woo S *et al* 2018 Current-driven dynamics and inhibition of the skyrmion Hall effect of ferromagnetic skyrmions in GdFeCo films *Nat. Commun.* **9** 959

[121] Brandao J, Dugato D A, Dos Santos P and Cezar J C 2019 Evolution of zero-field ferrimagnetic domains and skyrmions in exchange-coupled Pt/CoGd/Pt confined nanostructures: implications for antiferromagnetic devices *ACS Appl. Nano Mater.* **2** 7532
[122] Roy P E, Otxoa R M and Moutafis C 2019 Controlled anisotropic dynamics of tightly bound skyrmions in a synthetic ferrimagnet due to skyrmion deformation mediated by induced uniaxial in-plane anisotropy *Phys. Rev.* B **99** 094405
[123] Khoshlahni R, Lepadatu S, Kouhi M and Mohseni M 2023 Skyrmion dynamics induced by surface acoustic waves in antiferromagnetic systems *Phys. Rev.* B **107** 144421
[124] Puebla J, Hwang Y, Maekawa S and Otani Y 2022 Perspectives on spintronics with surface acoustic waves *Appl. Phys. Lett.* **120** 220502
[125] Weiler M, Dreher L, Heeg C, Huebl H, Gross R, Brandt M S and Goennenwein S T B 2011 Elastically driven ferromagnetic resonance in nickel thin films *Phys. Rev. Lett.* **106** 117601
[126] Dreher L, Weiler M, Pernpeinter M, Huebl H, Gross R, Brandt M S and Goennenwein S T B 2012 Surface acoustic wave driven ferromagnetic resonance in nickel thin films: theory and experiment *Phys. Rev.* B **86** 134415
[127] Thevenard L, Duquesne J-Y, Peronne E, von Bardeleben H J, Jaffres H, Ruttala S, George J-M, Lemaître A and Gourdon C 2013 Irreversible magnetization switching using surface acoustic waves *Phys. Rev.* B **87** 144402
[128] Thevenard L, Camra I S, Prieur J-Y, Rovillain P, Lemaître A, Gourdon C and Duquesne J-Y 2016 Strong reduction of the coercivity by a surface acoustic wave in an out-of-plane magnetized epilayer *Phys. Rev.* B **93** 140405(R)
[129] Dean J, Bryan M T, Cooper J D, Virbule A, Cunningham J E and Hayward T J 2015 A sound idea: manipulating domain wall in magnetic nanowires using surface acoustic waves *Appl. Phys. Lett.* **107** 142405
[130] Edrington W, Singh U, Dominguez M A, Alexander J R, Nepal R and Adenwalla S 2018 SAW assisted domain wall motion in Co/Pt multilayers *Appl. Phys. Lett.* **112** 052402
[131] Adhikari A and Adenwalla S 2021 Surface acoustic waves increase magnetic domain wall velocity *AIP Adv.* **11** 015234
[132] Adhikari A, Gilroy E R, Hayward T J and Adenwalla S 2021 Surface acoustic wave assisted depinning of magnetic domain walls *J. Phys.: Condens. Matter* **33** 31LT01
[133] Castilla D *et al* 2020 Magnetization process of a ferromagnetic nanostrip under the influence of a surface acoustic wave *Sci. Rep.* **10** 9413
[134] Wei Y, Li X, Gao R, Wu H, Wang X, Zeng Z, Wang J and Liu Q 2020 Surface acoustic wave assisted domain wall motion in [Co/Pd]2/Pd(t)/Py multilayers *J. Magn. Magn. Mater.* **502** 166546
[135] Cao Y, Bian X N, Yan Z, Xi L, Lei N, Qiao L, Si M S, Cao J W, Yang D Z and Xue D S 2021 Surface acoustic wave-assisted spin-orbit torque switching of the Pt/Co/Ta heterostructure *Appl. Phys. Lett.* **119** 012401
[136] Shuai J, Hunt R G, Moore T A and Cunningham J E 2023 Separation of heating and magnetoelastic coupling effects in surface-acoustic-wave-enhanced creep of magnetic domain walls *Phys. Rev. Appl.* **20** 014002
[137] Shuai J, Lopez-Diaz L, Cunningham J E and Moore T A 2023 Surface acoustic wave effect on magnetic domain wall dynamics *Phys. Rev.* B **108** 104420
[138] Chen C, Lin T, Niu J, Sun Y, Yang L, Kang W and Lei N 2022 Surface acoustic wave controlled skyrmion-based synapse devices *Nanotechnology* **33** 115205
[139] Chen R, Chen C, Han L, Liu P, Su R, Zhu W, Zhou Y, Pan F and Song C 2023 Ordered creation and motion of skyrmions with surface acoustic wave *Nat. Commun.* **14** 4427
[140] Shuai J, Moore T A, Lopez-Diaz L and Cunningham J E 2024 Transport of skyrmions by surface acoustic waves *Appl. Phys. Lett.* **124** 202407
[141] Nepal R, Güngördü U and Kovalev A A 2018 Magnetic skyrmion bubble motion driven by surface acoustic waves *Appl. Phys. Lett.* **112** 112404
[142] Yokouchi T, Sugimoto S, Rana B, Seki S, Ogawa N, Kasai S and Otani Y 2020 Creation of magnetic skyrmions by surface acoustic waves *Nat. Nanotechnol.* **15** 361
[143] Miyazaki Y, Yokouchi T and Shiomi Y 2023 Trapping and manipulating skyrmions in two-dimensional films by surface acoustic waves *Sci. Rep.* **13** 1922
[144] Chen C, Wei D, Sun L and Lei N 2023 Suppression of skyrmion Hall effect via standing surface acoustic waves in hybrid ferroelectric/ferromagnetic heterostructures *J. Appl. Phys.* **133** 203904
[145] Yang Y *et al* 2024 Acoustic-driven magnetic skyrmion motion *Nat. Commun.* **15** 1018
[146] Sun J, Zhao Y, Shi S, Zhang Y and Wang J 2022 Motion of a magnetic skyrmionium driven by acoustic wave *Appl. Phys. Lett.* **121** 242406
[147] Prasad B *et al* 2020 Ultralow voltage manipulation of ferromagnetism *Adv. Mater.* **32** 2001943
[148] Huang Y-L *et al* 2020 Manipulating magnetoelectric energy landscape in multiferroics *Nat. Commun.* **11** 2836